Solar Energy Materials & Solar Cells 95 (2011) 1819–1825

Contents lists available at ScienceDirect

Solar Energy Materials & Solar Cells

journal homepage: www.elsevier.com/locate/solmat

Nanostructured hematite photoelectrochemical electrodes prepared by the low temperature thermal oxidation of iron

Pritesh Hiralal [a,*], Sina Saremi-Yarahmadi [b], Bernhard C. Bayer [a], Haolan Wang [a], Stephan Hofmann [a], K.G. Upul Wijayantha [c], Gehan A.J. Amaratunga [a]

[a] Department of Enginering, University of Cambridge, 9 JJ Thomson Avenue, Cambridge, CB30FA, UK
[b] Department of Materials, University of Loughborough, Loughborough, LE11 3TU, UK
[c] Department of Chemistry, University of Loughborough, Loughborough, LE11 3TU, UK

ARTICLE INFO

Article history:
Received 20 May 2010
Received in revised form
11 January 2011
Accepted 31 January 2011
Available online 18 February 2011

Keywords:
Iron oxide
Photoelectrochemical
Hydrogen
Thermal oxidation
Nanostructure

ABSTRACT

We report on a facile low temperature method for the preparation of high surface area, nanostructured α-Fe_2O_3 (hematite) thin films and their application as photoelectrochemical (PEC) water splitting electrodes. The hematite films are fabricated by thermal oxidation in air of DC sputter deposited iron films at temperatures as low as 255 °C. This method results in films with a higher surface area than typically obtained by directly sputtering α-Fe_2O_3. It is shown that beyond a minimum iron thickness, α-Fe_2O_3 nanowires result upon thermal treatment in atmospheric conditions. Structural and optical characteristics of the resulting films are analyzed. The oxidation process is studied in detail and correlated to the photoelectrical properties. The Fe films oxidize in stages via Fe-oxide layers of increasing oxidation states. Resulting photoelectrochemical performance of fully oxidized films is a balance between optical absorption and charge collection, which varies with film thickness. The optimum film achieved a net photocurrent density of 0.18 mA/cm^2 in 1 M NaOH at 1.23 V vs. RHE under simulated AM1.5 sunlight, amongst the highest values reported for undoped hematite films produced at low temperature.

1. Introduction

The direct photoelectrolysis of water, the process whereby light illuminating a semiconductor is used to split water into its basic components, hydrogen and oxygen, brings the promise of a clean, renewable energy source, hydrogen, which overcomes the current hurdles of intermittency, portability and usage on demand.

Since Fujishima and Honda [1] demonstrated the photoelectrochemical effect in TiO_2 in 1972, significant work has been conducted to search for suitable materials which could effectively carry out this reaction. However, achieved efficiencies have as yet been much lower than expected. There are several basic material requirements to achieve this goal. Firstly, the bandgap of the semiconducting material should be small enough to allow for the collection of a sizeable portion of solar photons, but large enough to allow the reaction to occur ($\sim > 1.6$ eV). Secondly, to avoid any external bias, the position of the band edges should be matched to the redox potentials for the water dissociation. And finally, the material should be thermodynamically stable in water. Unfortunately, semiconductors with a bandgap small enough for the efficient collection of light have been unstable to photocorrosion [2].

Hematite (α-Fe_2O_3) is a candidate material, which offers a good compromise. With a bandgap of 2.1 eV (considerably smaller than 3.2 eV for TiO_2), it absorbs a good proportion of sunlight and yet has good electrochemical stability. It has a number of additional properties, which make it particularly attractive for water splitting applications; namely low cost, abundance and non-toxicity. However, PEC performance of hematite photoelectrodes has been much below its theoretical maximum of 12.9% [3]. This is attributed to its short minority carrier diffusion length [4], as well as a rapid falloff in the absorption cross-section of the material for wavelengths approaching the bandgap value [5]. In addition, the conduction band edge is too positive to reduce water to hydrogen directly. This can be overcome by applying a bias, which may be provided by another solar cell in a tandem configuration [2].

Several approaches have been taken to tackle the low mobility and hence improve PEC performance of hematite electrodes. Broadly speaking, these can be divided into 2 types: doping (to improve the conductivity of hematite) and structural enhancement (to increase the surface area and reduce the distance photogenerated charge carriers have to travel for collection).

* Corresponding author.
E-mail addresses: pv237@cam.ac.uk (P. Hiralal), s.saremi@lboro.ac.uk (S. Saremi-Yarahmadi).

0927-0248/$ - see front matter © 2011 Elsevier B.V. All rights reserved.
doi:10.1016/j.solmat.2011.01.049

There have been numerous attempts to improve the PEC performance of hematite electrodes by doping. Only a few dopants, Ti [6,4], Si [7,8], Mo [9] and Pt [10], have resulted in enhanced performance, and this has been dependent on the preparation technique. Kay et al. [8] showed a 65% enhancement upon doping with Si leading to photocurrent of 2.2 A/cm^2 at 1.23 V vs. RHE. However, the exact influence of dopants on carrier mobility remains poorly understood. The improvement is generally attributed both to the change in charge carrier concentration and better conductivity as well as the effect the dopant on the film morphology, leading to smaller features in the film.

On the other hand, several attempts have been made to modify the film morphology to overcome the short hole diffusion length (<5 nm) [4]. Unlike TiO_2, nanostructured hematite electrodes based on interconnected spherical particles (50 nm diameter) have shown high charge-carrier recombination losses and very low photocurrent efficiency [11]. Hematite nanorods have been grown directly on FTO substrates by hydrothermal growth [12] and on iron foils or wires by thermal oxidation [13–15]. Nanorods or nanowires (NWs) result in a high surface area at the semiconductor/electrolyte interface, a short diffusion distance for holes, and a direct conduction path for electrons, free of grain boundaries. Anodized hematite films with very porous structures have also been used [16]. Recently, intentional structural enhancement and formation of hematite nanotubes has been reported, which resulted in improvements in PEC performance of hematite films, compared with equivalent planar films, but overall photocurrents remain low [17].

Sputter deposition is a well known technique for producing controllable, reproducible films and hematite films produced with this method have been studied before as electrodes, although performance has typically been low (<1 μA/cm^2) for undoped films [5]. It has been recently shown that by post-thermally oxidizing a sputter deposited iron film, it is possible to obtain high surface area hematite surfaces (e.g. with NWs) [13,18].

With a view of exploiting the enhanced surface resulting from this simple technique in photoelectrochemical cells, we study the oxidation process, providing some insight on the development of oxidation, and correlate this to the resulting photoelectrochemical performance, leading to an insight into efficiency limiting factors in hematite films. Nanostructured films were achieved by oxidizing iron films in air at temperatures as low as 255 °C. The low temperature used in this method allows the use of less temperature tolerant substrates such as indium tin oxide (ITO) and, potentially, flexible substrates.

2. Method

2.1. Thin film preparation

1×2 cm^2 conductive fluorine-doped tin oxide (FTO–TEC 8, Pilkington, 8 Ω/square) glass substrates (0.5 cm thick) were cleaned ultrasonically in acetone, isopropanol and deionized water in the given order, and dried under nitrogen flow. Iron was subsequently sputter deposited onto the cleaned substrates using direct current magnetron sputtering (DC sputtering). The sputtering chamber was pumped down to a base pressure of $\sim5\times10^{-6}$ mbar. Deposition was conducted at a power of 100 W, under Ar flow at a pressure of 3.5×10^{-3} mbar for varying lengths of time, resulting in a deposition rate of 4–6 nm/min. Films in the range of 20–220 nm where sputtered. Oxidation of the sputtered films was then carried out in air by placing the sample on a hotplate for different durations. Temperature of the iron face was maintained at ~255 °C measured by a *k*-type thermocouple in contact with the surface of the FTO substrate.

2.2. Structural characterization

Nanostructure and surface morphology was investigated by field emission scanning electron microscopy (FE SEM) (Philips XL30, operated at 5 kV). Thickness of the films, before and after oxidation where measured by surface profilometry (Sloan Dectak). The phase and crystallinity of deposited films on microscope glass slides (soda glass) and FTO were characterized using X-ray diffraction (XRD), measured with a Philips PW1730 diffractometer (Cu-Kα radiation 1.54060 Å). Raman spectroscopy of iron oxide films on FTO glass was carried out in a Renishaw Raman spectrometer using an excitation wavelength of 633 nm. A minimum of three spots per sample were measured to ensure homogeneity. The crystallinity of individual NWs was determined by transmission electron microscopy using a FEI Tecnai 20 microscope operating at 200 kV.

2.3. Optical and photoelectrochemical measurements

Optical absorption measurements were performed using a Lambda 35 Perkin-Elmer UV–vis spectrophotometer. Photocurrent response was measured using a three-electrode configuration in 1 M NaOH electrolyte, Ag/AgCl/KCl as the reference electrode, and a platinum wire as the counter electrode. The potential of the photoelectrode was controlled by a potentiostat (microAutoLab, type III) and is reported against the reversible hydrogen electrode (RHE). In the electrochemical cell, light enters through a quartz window and travels about a 5 mm path length in the electrolyte before illuminating the photoelectrode. The Fe_2O_3 electrode was illuminated through electrolyte side, and illumination area was 1 cm^2. The illumination source was an AM 1.5 class A solar simulator (Solar Light 16S—300 solar simulator) equipped with a 300 W xenon lamp. The intensity of the light was calibrated at 1000 W/m^2 using a class II pyranometer (PMA2144, Solar Light Co., Inc.) equipped with a digital photometer (PMA2100, Solar Light Co., Inc.).

The incident photon to current conversion efficiency (IPCE) was obtained by measuring the incident photon flux of a 75 W xenon lamp connected to a monochromator (TMc300, Bentham Instruments Ltd.). The light was calibrated using a silicon diode. Photocurrent spectra were measured at 0.23 V vs. Ag/AgCl. Readings were collected every 5 nm as the monochromated light was scanned from 320 to 650 nm.

3. Results and discussion

Fig. 1(A)–(E) shows SEM images of the surface of iron films of various thicknesses after being oxidized in air for 24 h at 255 °C. In all cases, the resulting surface has a granular morphology with 50–150 nm particles. Beyond a certain thickness (>45 nm), NW formation can be observed even at this low temperature. NW density increases with thickness up to a certain point after which it remains roughly constant. Oxide NW formation consists of both flat sword-shaped platelets and thin wires of constant width, both of which are commonly observed in hematite NW formation by thermal oxidation at higher temperatures [13,14,19]. Fig. 1(F) shows a photograph of a fully oxidized 115 nm iron film. Film color is indicative of the presence of hematite [20].

Film thicknesses quoted refer to the as-deposited iron film. Due to the oxygen intake and the lower density of α-Fe_2O_3 compared to Fe metal, a thickness increase of about 90% is observed upon full oxidation. Fig. 2(A) shows the thickness relation between the original iron and the oxidized films. Fig. 2(B) shows a TEM image of a single wire (diameter ~10 nm). The selected area electron diffraction (SAED) pattern in

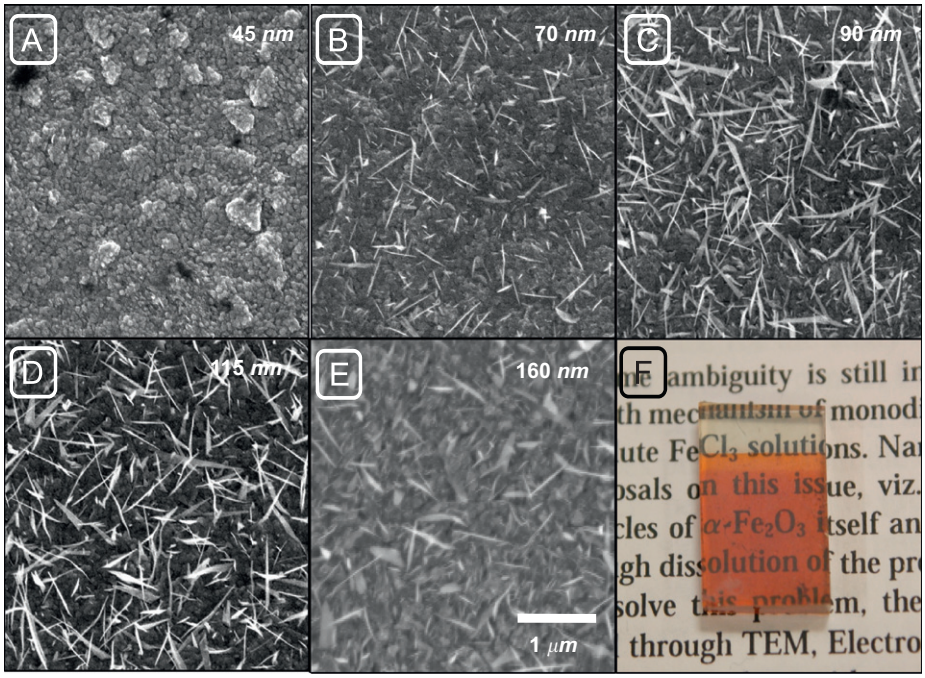

Fig. 1. (A)–(E) Set of SEM images of the iron oxide films resulting from annealing a set of iron films of varying thicknesses at 255 °C for 24 h in air. Film thicknesses quoted refer to the initial iron film, before oxidation. (f) Photograph of a fully oxidized 115 nm iron film.

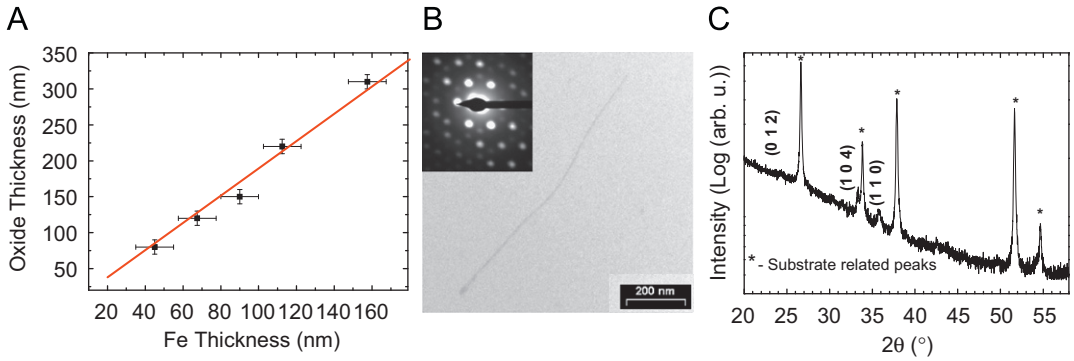

Fig. 2. (A) Iron to iron oxide film thickness relation. (B) TEM image of a single NW. Inset shows the selected area electron diffraction (SAED) pattern showing a crystalline hematite NW. (C) Typical XRD pattern of an oxidized film.

the inset reveals a crystalline structure of rhombohedral α-Fe_2O_3, with a measured d spacing of 2.72 Å, in good agreement with the (1 0 4) interplanar spacing. This is surprising given that the crystallization temperature for hematite is >390°C [21]. The XRD diffractogram of the bulk film, Fig. 2(C), shows very weak (1 0 4) and (1 1 0) hematite reflections, consistent with the poor crystallization expected at this temperature.

A systematic study was performed in order to understand the oxidation process and determine the optimum parameters for photoelectrochemical applications. The structural changes of the films were studied using Raman spectroscopy. Fig. 3(A) shows the Raman spectra of the films shown in Fig. 1, various iron films of increasing thickness annealed for 24 h at 255 °C. The presence of hematite in all these annealed films irrespective of thickness is confirmed, since the typical Raman peaks of hematite [22,23,24], labeled "H" in Fig. 3(A), are found in all scans. However, on thicker films we also find an additional broad peak around $\sim$660 cm^{-1}. The intensity of this peak relative to the hematite peaks increases with increasing film thickness. This $\sim$660 cm^{-1} peak is found in the Raman spectra of three non-hematite iron oxide phases, namely magnetite (Fe_3O_4), maghemite (γ-Fe_2O_3) and wustite (FeO) [22,23,24]. Specific assignment which of these phases are present in the thicker films remains ambiguous due to the lack of additional, lower intensity, corresponding peaks in the spectra [22,23,24]. However, we can conclude that the thin films consist of practically pure hematite after annealing, whereas with increasing film thickness non-hematite oxide phases are increasingly present as well.

Hematite is a fully oxidized form and the most stable of the iron oxides. There are generally 2 known routes for the formation of hematite from Fe: the hydroxide route, where hematite formation occurs via an iron hydroxide and the oxide route, in which the oxidation state of Fe gradually increases, yielding oxide layers with increasing oxidation, i.e. via magnetite (Fe_3O_4) and maghemite (γ-Fe_2O_3) [24]. Although it is not possible to determine the exact phase of the non-hematite oxides from our Raman data, we can exclude the presence of hydroxides [22,23,24]. This suggests the oxidation in our films occurs via the oxide route.

Color change of the film during the oxidation process can be observed by the naked eye. Whilst thinner metallic iron films soon

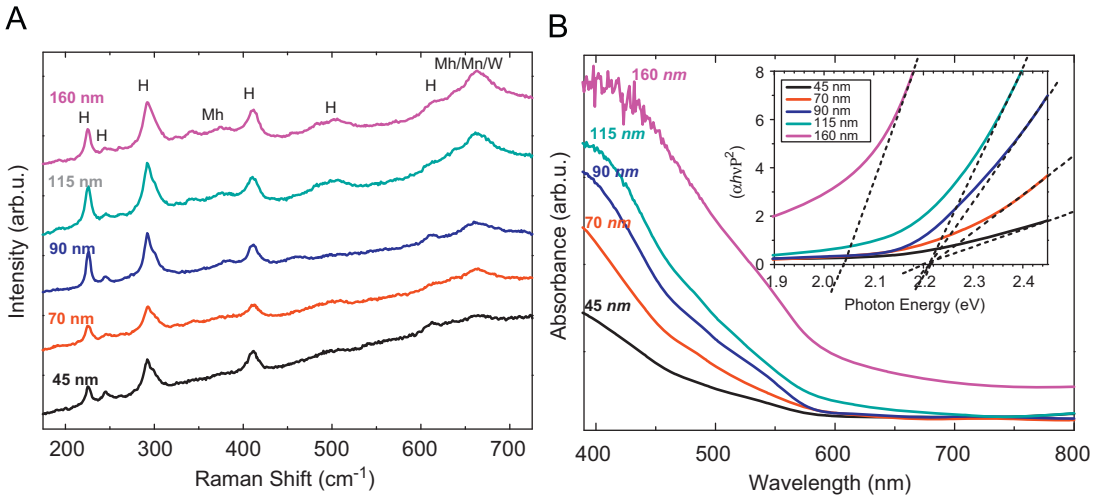

Fig. 3. (A) Raman spectra and (B) optical absorption spectra of the samples of varying Fe thickness and constant annealing time (24 h). "H" corresponds to Raman peaks of hematite, while "Mh", "Mn" and "W" represent peak positions, which can be ascribed to maghemite, magnetite or wustite, respectively.

turn into a homogeneous transparent orange/brown (typically correlated to hematite), thicker films take a longer time (~few days) to reach this color, and the films typically soon turn brown/black (indicative of magnetite/maghemite) with patches gradually changing to the hematite orange/brown [20]. Optical absorption spectra are shown in Fig. 3(B). As expected, absorption increases with film thickness. The inset shows Tauc plots for bandgap calculation. With exception of the thickest film, the bandgap is constant throughout the samples, 2.21 eV, consistent with reported values for hematite. The thickest film (160 nm) shows a bandgap of 2.04 eV. Although this is still within reported values for hematite, given the bandgap shifts to 2.2 eV upon further annealing and the observed color of the film, we propose a more accurate match to maghemite (γ-Fe_2O_3), an n-type semiconductor with bandgap 2.03 eV [24]. Maghemite is isostructural with magnetite, and generally results from a topotactic transformation from magnetite upon further oxidation. This observation fits with the hypothesis of hematite formation via lower oxidation state phases.

To further investigate the oxidation process and confirm the hypothesis that thermally oxidized films oxidize via the magnetite/maghemite route, Raman spectra of several films were measured as a function of annealing time, shown in Fig. 4. As-deposited films show a very weak signal at 660 cm^{-1} ascribed to the slow oxidation occurring in the presence of air at room temperature. Upon annealing, the relatively thin films (~40 nm) show strong hematite peaks and a relatively weak 660 cm^{-1} peak even after short anneals. This does not change significantly with further annealing time (Fig. 4(a)). This suggests rapid oxidation to the hematite phase. In contrast, on thicker films (Fig. 4(b)), a sizeable non-hematite peak can be observed after short annealing times, with its relative intensity decreasing slowly with annealing time. This corresponds to a gradual increase of oxidation within the film, and suggests diffusion limited formation of the oxide layers, most likely limited by the diffusion of oxygen into the bulk of the film. This observation is supported by results from a recent report in which the profile of a thermally oxidized bulk iron wire was analyzed to find layers of subsequently lower oxidation state with depth [15]. Note that, in contrast, the formation of the oxide NWs on the surface is likely governed by a different, more complex Fe diffusion mechanism [25]. UV–vis absorption spectra of the same films (not-shown) show no variation with time on the thin case, and similarly to before, broadband absorption until the sample was homogeneously oxidized and hematite is predominant.

Fig. 5(a) shows the PEC performance of a set of illustrative films; various thicknesses annealed for 8 h. The maximum photocurrent density, 180 μA at 0.23 V vs. Ag/AgCl (1.23 V vs. RHE), is achieved for a 40 nm film. Further annealing beyond full oxidation (varies depending on film thickness) results in a consequent drop in the photocurrent density.

Incident photon to current efficiency (IPCE) values obtained for an optimum and a thick sample are shown in Fig. 5(b). A quantum efficiency of over 7% at 350 nm is obtained for the 40 nm-thick sample. 350 nm light has a very short penetration depth in hematite, in the order of a few nanometers. This is similar to the hole diffusion length in hematite (~2–4 nm). Hence, the holes generated from short wavelength light do not need to diffuse too far in order to reach the hematite/electrolyte interface, and are more effectively collected. The relatively higher quantum efficiency may be attributed to this, as well as the excess energy provided to the carriers by higher energy photons.

Considering that the light absorption coefficient of α-Fe_2O_3 at 450 nm is 2.3×10^5 cm^{-1} [4,20], resulting in a light penetration depth of ~43 nm; it can be said that it is only the top 40–50 nm of a flat hematite film which absorbs useful light, and material beyond this depth does not significantly contribute to light absorption and charge carrier generation. This leads to an optimum film thickness for photocurrent generation. Films which are too thin, lose useful light, while an increased thickness means photogenerated charge carriers need to travel longer before being collected, increasing recombination losses. This also explains the fact that the photocurrent onset occurs at lower photon energies in the thinner film (inset in Fig. 5(b)). Our results suggest that optimum PEC performance is achieved with an iron film thickness of ~40 nm. This corresponds to ~75 nm thick hematite, just slightly over that expected from our hypothesis. This can be justified by considering the nanostructured nature of our films, which is not formed by tightly packed bulk hematite which the penetration depth refers to. Additionally, the nanostructured surface aids absorption of light.

Poor hole transport to the semiconductor/electrolyte interface is one of the limiting factors for the efficient photo-response and photocatalytic activity of hematite photoanodes due to the short hole diffusion length of α-Fe_2O_3. It has been shown [26] that the increase in the particle size and coalescence of small particles resulted in a decrease of photocurrent density. Long annealing times result in further growth of grains of hematite and gradual disappearance of the fine nanostructure. This would diminish the

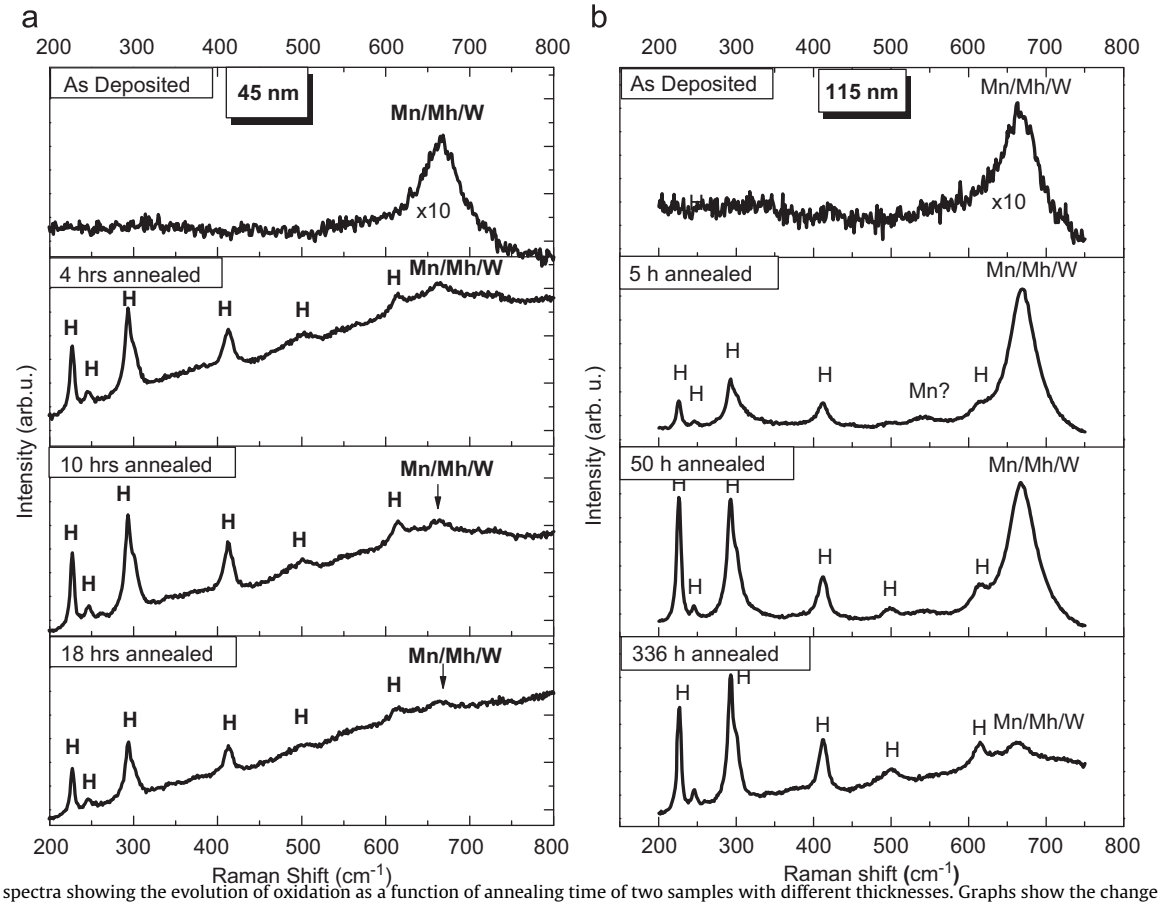

Fig. 4. Raman spectra showing the evolution of oxidation as a function of annealing time of two samples with different thicknesses. Graphs show the change in the Raman spectra of a (a) 45 nm (thin case (≈ 40–70 nm Fe)) and (b) 115 nm iron film (thick case (≥ 100 nm Fe)). ("H"—hematite, "Mh"—maghemite, "Mn"—magnetite, "W"—wustite related Raman peaks.)

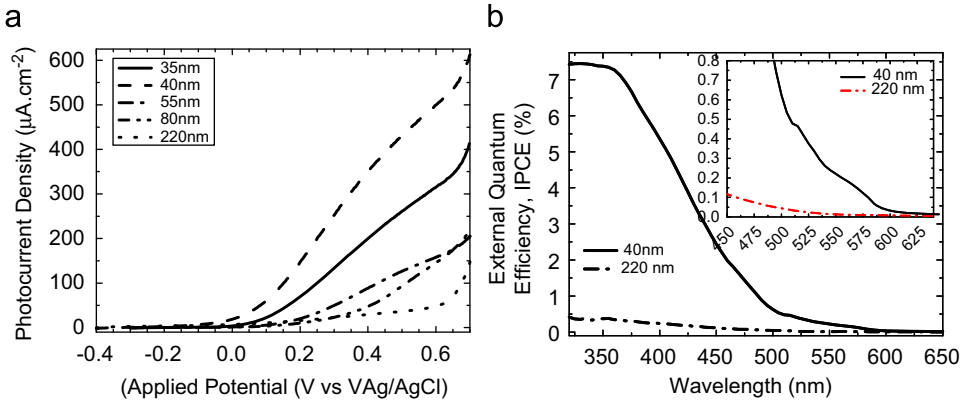

Fig. 5. (a) Photocurrent density of various film thicknesses annealed for 8 h and (b) IPCE characterization of Fe_2O_3 films. Two cases are shown: thin film (40 nm) and thick film (220 nm).

PEC performance by the formation of larger surface features, resulting in a reduced active surface area as well as an increased path length for holes to reach the surface. As a result, most of the photogenerated holes recombine before reaching the interface. This view is supported by the observation of decaying photocurrent with longer annealing times. The trends described above are shown qualitatively in Fig. 6(a), which shows the resulting photocurrent as a function of annealing time and film thickness. The 3D mesh is fitted to discrete experimental data points shown.

From this data we devise a model (Fig. 6(b)) to explain the iron oxidation process and correlate the state of oxidation to the photoelectrical performance. We propose Fe oxidizes gradually, and oxidation occurs from the surface towards the inner side of the film, as limited by oxygen diffusion.

Upon annealing, hematite, the most thermodynamically stable iron oxide, forms early on (within a few minutes) the surface, where oxygen is most easily accessible (A). At this stage, the PEC response is good, as charge transfer occurs straight from hematite to Fe metal. On a very thin film, full oxidation occurs very rapidly. On thicker films, the formation of hematite beneath the already oxidized layer relies on the diffusion of oxygen through the top oxide layer, leading to longer times required for the complete oxidation. Given diffusion of oxygen through Fe is a slow process, oxidation occurs in phases, via the $Fe_3O_4 \rightarrow \gamma\text{-}Fe_2O_3 \rightarrow \alpha\text{-}Fe_2O_3$ route [24,15]. These phases pose a barrier

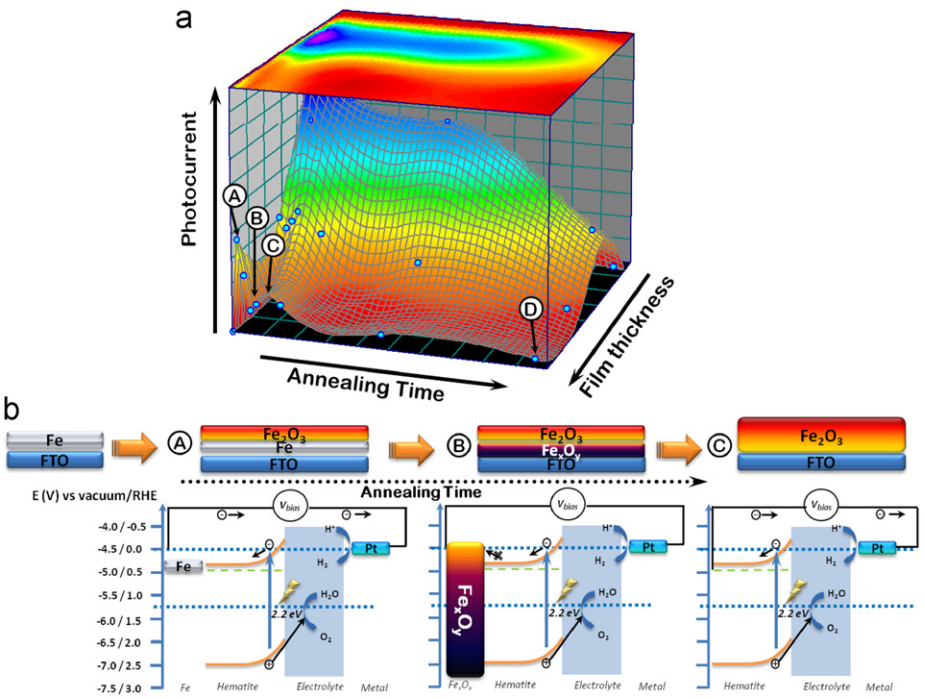

Fig. 6. (a) Qualitative schematic showing the photocurrent as a result of varying deposition and annealing conditions. Curve generated by fitting onto discrete measured points. (b) Proposed model for the development of oxidation of iron upon thermal oxidation and its relation to the films photoelectrochemical properties.

for charge transfer, resulting in a degraded PEC performance (B). Further annealing eventually fully oxidizes the whole film, removing the barrier, and improving photocurrent (C). The annealing times have to be adjusted in such a way that the optimum effective thickness of oxidized film is obtained while the damage to the fine nanostructure of the surface of the film is minimized. Although long annealing times results in further oxidation of the film it causes the grain growth and consequently the collapse of fine nanostructure (D).

4. Conclusion

Iron oxide films obtained by thermally oxidizing sputter coated iron films at low temperatures (~255 °C) have been studied as candidates for photoelectrochemical cells. A parametric study has been conducted in order to optimize film thickness and annealing conditions, leading to an insight into the thermal oxidation process in iron and optimum conditions for hematite PEC cells. Thermally oxidized films show a distinct crystalline nanostructured morphology, and a superior performance compared to other sputtered hematite films, 0.18 mA/cm^2 at 1.23 V vs. RHE. This opens up a possible route for the production of PEC cells under mild conditions, tolerating a larger number of substrates. Whether the higher surface area resulting from this method is responsible for the enhancement remains yet an open question. Although the higher photocurrents obtained would be a positive indication, other parameters such as film thickness and grain formation have also been optimized as compared to previous works. It is suggested that it is the optimum thickness of the oxidized film together with the retained nanostructure at short annealing times, which contributes to good PEC performance of the thin films. This work defines some working parameters, which may serve as a baseline for further enhancement in hematite PEC cells. Further work is under progress to dope these films and to exploit the mild processing conditions of these films onto flexible substrates.

Acknowledgement

This work has been done through the Nokia–Cambridge University Strategic Research Alliance in Nanotechnology. We would like to acknowledge Dr. D. Hasko for his support and insightful discussions.

References

[1] A. Fujishima, K. Honda, Electrochemical photolysis of water at a semiconductor electrode, Nature 238 (1972) 37–38.
[2] M. Grätzel, Photoelectrochemical cells, Nature 414 (2001) 338–344.
[3] A. Murphy, P. Barnes, L. Randeniya, I. Plumb, I. Grey, M. Horne, J. Glasscock, Efficiency of solar water splitting using semiconductor electrodes, International Journal of Hydrogen Energy 31 (2006) 1999–2017.
[4] J.H. Kennedy, K.W. Frese, Photooxidation of water at alpha-Fe_2O_3 electrodes, Journal of Electrochemical Society 125 (1978) 709–714.
[5] J.A. Glasscock, P.R.F. Barnes, I.C. Plumb, N. Savvides, Enhancement of photoelectrochemical hydrogen production from hematite thin films by the introduction of Ti and Si, Journal of Physical Chemistry C 111 (November) (2007) 16477–16488.
[6] C. Jorand Sartoretti, B.D. Alexander, R. Solarska, I.A. Rutkowska, J. Augustynski, R. Cerny, Photoelectrochemical oxidation of water at transparent ferric oxide film electrodes, The Journal of Physical Chemistry B vol. 109 (Jul. 2005) 13685–13692.
[7] S. Saremi-Yarahmadi, K.G.U. Wijayantha, A.A. Tahir, B. Vaidhyanathan, Nanostructured α-Fe_2O_3 electrodes for solar driven water splitting: effect of doping agents on preparation and performance, The Journal of Physical Chemistry C 113 (2009) 4768–4778.
[8] A. Kay, I. Cesar, M. Grätzel, New benchmark for water photooxidation by nanostructured alpha-Fe_2O_3 films, Journal of the American Chemical Society 128 (Dec. 2006) 15714–15721.
[9] A. Kleiman-Shwarsctein, Y.-S. Hu, A.J. Forman, G.D. Stucky, W. McFarland, Electrodeposition of α-Fe_2O_3 doped with Mo and Cr as photoanodes for photocatalytic water splitting, Journal of Physics and Chemistry C 112 (2008) 15900–15907.
[10] Y.-S. Hu, A. Kleiman-Shwarsctein, A.J. Forman, D. Hazen, J.-N. Park, E.W. McFarland, Pt-doped α-Fe2O3 thin films active for photoelectrochemical water splitting, Chemistry of Materials 20 (2008) 3803–3805.
[11] U. Bjorkstbn, J. Moser, M. Gratzel, Photoelectrochemical studies on nanocrystalline hematite films, Chemistry of Materials 6 (1994) 858–863.
[12] N. Beermann, L. Vayssieres, S.-E. Lindquist, A. Hagfeldt, Photoelectrochemical studies of oriented nanorod thin films of hematite, Journal of The Electrochemical Society 147 (2000) 2456–2461.

[13] P. Hiralal, H.E. Unalan, K.G.U. Wijayantha, A. Kursumovic, D. Jefferson, G.A.J. Amaratunga, Growth and process conditions of aligned and patternable films of iron(III) oxide nanowires by thermal oxidation of iron, Nanotechnology 19 (2008) 455608–455614.
[14] X. Wen, S. Wang, Y. Ding, Z.L. Wang, S. Yang, Controlled growth of large-area, uniform, vertically aligned arrays of alpha-Fe_2O_3 nanobelts and nanowires, The Journal of Physical Chemistry B 09 (January) (2005) 215–220.
[15] A.G. Nasibulin, S. Rackauskas, H. Jiang, Y. Tian, P.R. Mudimela, S.D. Shandakov, L.I. Nasibulina, S. Jani, E.I. Kauppinen, Simple and rapid synthesis of α-Fe_2O_3 nanowires under ambient conditions, Nano Research 2 (2009) 373–379.
[16] H.E. Prakasam, O.K. Varghese, M. Paulose, G.K. Mor, C. a Grimes, Synthesis and photoelectrochemical properties of nanoporous iron (III) oxide by potentiostatic anodization, Nanotechnology 17 (2006) 4285–4291.
[17] S.K. Mohapatra, S.E. John, S. Banerjee, M. Misra, Water photoxidation by smooth and ultrathin α-Fe_2O_3 nanotube arrays, Chemistry of Materials 21 (2009) 3048–3055.
[18] T. Yu, Y. Zhu, X. Xu, K.-S. Yeong, Z. Shen, P. Chen, C.-T. Lim, J.T.-L. Thong, C.-H. Sow, Substrate-friendly synthesis of metal oxide nanostructures using a hotplate, Small (Weinheim an der Bergstrasse, Germany) 2 (2006) 80–84.
[19] R. Takagi, Growth of oxide whiskers on metals at high temperature, Journal of the Physical Society of Japan 12 (1957) 1212–1218.
[20] U. Schwertmann, R. Cornell, Iron Oxides in the Laboratory, Wiley-VCH, 2000, pp. 27–37.
[21] L. Vayssieres, N. Beermann, S.-E. Lindquist, A. Hagfeldt, Controlled aqueous chemical growth of oriented three-dimensional crystalline nanorod arrays: application to iron(III) oxides, Chemistry of Materials 13 (Feb. 2001) 233–235.
[22] D.L. a de Faria, S. Venâncio Silva, M.T. de Oliveira, Raman microspectroscopy of some iron oxides and oxyhydroxides, Journal of Raman Spectroscopy 28 (Nov. 1997) 873–878.
[23] S.J. Oh, D. Cook, H. Townsend, Characterization of iron oxides commonly formed as corrosion products on steel, Hyperfine Interactions 112 (1998) 59–66.
[24] R.M. Cornell, U. Schwertmann, The Iron Oxides, Wiley-VCH, 2003, pp. 126–127 and 146–158.
[25] D. a Voss, E.P. Butler, T.E. Mitchell, The growth of hematite blades during the high temperature oxidation of iron, Metallurgical Transactions A 13 (May) (1982) 929–935.
[26] S. Saremi-Yarahmadi, B. Vaidhyanathan, K.G.U. Wijayantha, Microwave-assisted low temperature fabrication of nanostructured α-Fe_2O_3 electrodes for solar-driven hydrogen generation, International Journal of Hydrogen Energy 35 (2010) September 10155–10165.